Hindawi Publishing Corporation
Journal of Nanomaterials
Volume 2008, Article ID 329601, 12 pages
doi:10.1155/2008/329601

Review Article

Atomic Layer Thermopile Materials: Physics and Application

P. X. Zhang[1,2] and H.-U. Habermeier[1,2]

[1] *Institute of Advanced Materials for Photoelcetrons, Kunming University of Science and Technology, Kunming 650051, China*
[2] *Max-Planck-Institut für Festkörperforschung, D-70569 Stuttgart, Germany*

Correspondence should be addressed to P. X. Zhang, pxzhang@fkf.mpg.de

Received 20 August 2007; Accepted 16 May 2008

Recommended by Donglu Shi

New types of thermoelectric materials characterized by highly anisotropic Fermi surfaces and thus anisotropic Seebeck coefficients are reviewed. Early studies revealed that there is an induced voltage in high T_C oxide superconductors when the surface of the films is exposed to short light pulses. Subsequent investigations proved that the effect is due to anisotropic components of the Seebeck tensor, and the type of materials is referred to atomic layer thermopile (ALT). Our recent studies indicate that multilayer thin films at the nanoscale demonstrate enhanced ALT properties. This is in agreement with the prediction in seeking the larger figure of merit (ZT) thermoelectric materials in nanostructures. The study of ALT materials provides both deep insight of anisotropic transport property of these materials and at the same time potential materials for applications, such as light detector and microcooler. By measuring the ALT properties under various perturbations, it is found that the information on anisotropic transport properties can be provided. The information sometimes is not easily obtained by other tools due to the nanoscale phase coexistence in these materials. Also, some remained open questions and future development in this research direction have been well discussed.

1. INTRODUCTION

The experiment of laser-induced voltage (LIV) effect, in which the $YBa_2Cu_3O_{7-\delta}$ (YBCO) thin films were used as a photosensor, was performed firstly by Chang et al. [1]. It was found that there is an induced voltage when pulsed laser light on the surface of YBCO thin films. It is proved that this LIV signal is induced by a thermoelectric anisotropy in the high T_C superconductor (HTSC) oxides [2–5]. These films absorb incident laser radiation, the top surface of thin film is heated rapidly, and an instant temperature difference between the top and bottom parts of the films is generated. This temperature gradient produces an electric voltage through the difference between components of the Seebeck tensor. This anisotropy in thermoelectricity originates from the anisotropic shape of the Fermi surface, causing the different properties of atomic layers in the HTSC oxides with low and high conductivity.

They behave like the two metals of a thermocouple. Therefore, these materials are called atomic layer thermopile (ALT). LIV signals become even larger if the films are grown on vicinal cut substrates because the vicinal cut structure offers more atomic layer junctions upon the interface. Figure 1 shows the typical time response of an induced voltage with incident pulsed laser of duration of 20 nanoseconds. The first quantitative description of this phenomenon was due to Lengfellner et al. [3], subsequently these signals observed in the ALT materials were defined as laser induced thermoelectric voltages (LITVs). Since then several high T_C superconductor oxides such as doped YBCO, $Bi_2Sr_2CaCu_2O_8$, $Tl_2Ba_2CaCu_2O_8$, and so forth have been studied and all of them have shown a similar effect [6–8]. Based on these studies, light detection devices have been designed [9–13], this demonstrates some superior characteristics over traditional bolometer and photon counting devices. Most obvious advantages are that the device can function over a broad spectral range at room temperature, has a fast time response and no applied bias is required.

In 1998, Habermeier et al. observed a similar effect in thin films of the quasicubic $La_{0.67}Ca_{0.33}MnO_3$ grown on vicinal cut substrates [14, 15]. This discovery showed that the ALT property is not confined to HTSC oxide materials, but subsists in other materials. On the other hand, Lanthanum manganites, which are interesting for their colossal magnetoresistance (CMR) properties, have attracted a lot of attention both from the viewpoint of

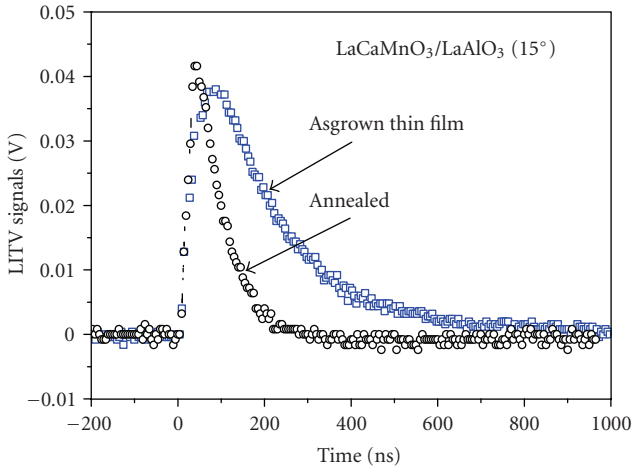

FIGURE 1: Typical laser induced voltage responses from the as-grown and annealed $LaCaMnO_3$ thin films grown on 15° tilted $LaAlO_3$ substrates, respectively.

basic physics as well as potential applications. The discovery extends the field of application and also provides new insight for the understanding the discipline of "strong-correlated electrons."

The LITV signal observed in ALT materials may be a general effect, and it has been well conscious of that the effect can be applied on several devices. However, there is no detailed relation between correlative macroscopic parameters of the used materials and the device performances. We derived a new formula based on a plane heat source and a thermal diffusion model [12]. This new formula does not only correlate the used material parameters with the device performances, but also facilitate the interpretation of physical mechanism of ALT materials.

Recently, several new ALT materials were reported, which belong to members of Ruddlesden-Popper family [15, 16]. Due to their different physical properties, they are suited to function at different spectral ranges or time responses. A new experiment shows that the superlattice like multilayer thin films grown on vicinal cut substrates demonstrate enhanced LITV signals. We will discuss these new ALT materials in detail in Section 3.

The first application of ALT materials is in light detection with advantages of fast time and broad spectral response, operating at room temperature, with no bias required. Based on the reverse effect, the Peltier effect, one can design microcooler. Examples and device design consideration will be given in Section 4.

The LITV measurements of HTSC and CMR thin films provide some important microscopic information on these materials. The direct information obtained is the anisotropy of the Seebeck coefficients, which are valuable for studying the transport property. In strongly correlated electronic system, like HTSC and CMR, currently the discussion has the focus on the nature of the phase coexistence. The measured LITV signals from HTSC and CMR are very sensitive to the doping, strain, oxygen content, charge- and orbital ordering,

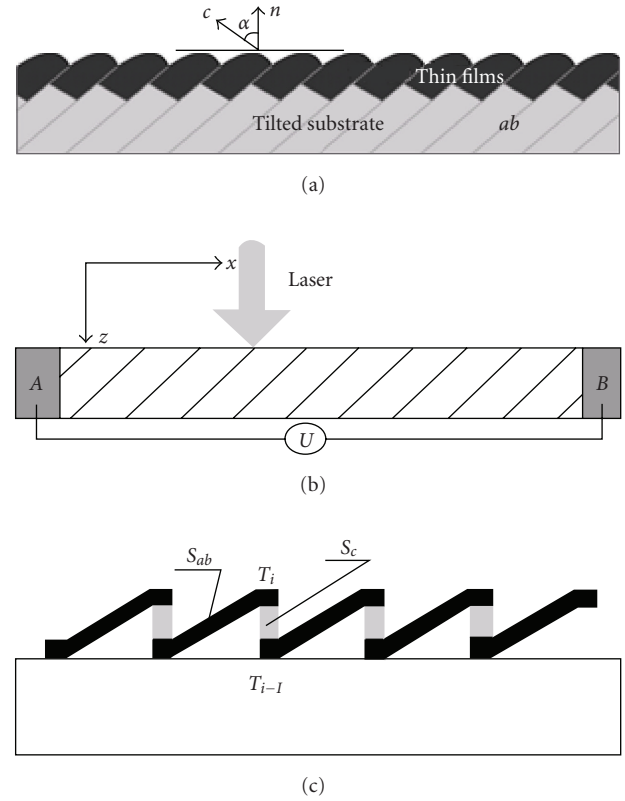

FIGURE 2: (a) The atomic layer thermopile thin film structure and the related coordinators. (b) The configuration of the samples used in the LITV measurements. (c) The schematic atomic layer thermopile model.

as well as the external perturbations such as the temperature, the applied magnetic field, and pressure. The information on anisotropic transport in these materials is regarded as being very important and hard to obtain through other experimental methods.

Although the ALT model and the transport mechanism of CMR materials have been well established, a number of questions in these studies are still needed to be answered, for example, why do CMR thin films exhibit anisotropic Seebeck effect even they are mostly cubic and in a paramagnetic phase, are there other materials which contain even larger ALT property? These open questions will be summarized at the end of this paper.

2. BASIC PRINCIPLES

A thermoelectric field E in a crystal can be induced by a temperature gradient ΔT:

$$E = S \cdot \Delta T, \tag{1}$$

where S is Seebeck tensor. For a thin film grown on vicinal cut substrate (See Figure 2(a)), illuminated by a laser pulse on the surface, a temperature gradient ΔT in z-direction is generated causing an induced voltage signal along the x-direction (U_x) due to the nonvanishing off-diagonal components of the Seebeck tensor. Based on the

experimental observations in $YBa_2Cu_3O_{7-\delta}$, Lengfellner et al. derived a formula according to (1) [3] as follows:

$$Ux = \frac{1}{2d}(S_{ab} - S_c)\sin(2\alpha)\overline{\nabla}_z T, \tag{2}$$

where $S_{ab} - S_c$ is the difference of the Seebeck coefficients in the *ab* plane and *c* direction of YBCO, respectively. *l* and *d* are the illuminated length and thickness of the film, α is the angle between the surface normal and *c*-axis of the substrate, *ZT* the temperature difference between the top and bottom part of the film. With this formula, one can explain most of the observed experimental facts, and also identify the nature of a laser-induced thermoelectric voltage from other photoinduced effect experimentally. According to this formula, the key factor is $S_{ab} - S_c$, that is, the anisotropy of Seebeck coefficient. Large transport anisotropy implies large induced voltage. It is well known that the properties of atomic layers in $YBa_2Cu_3O_7$ are very different: the CuO_2 layer is highly conductive, while the Y(Ba)-O layer has a low conductivity, as well as the Seebeck coefficients. Each two atomic layers form a junction like the thermocouple. If the thin films are grown on vicinal cut substrate, numerous of junction structures, which seem as the series thermocouples, form spontaneously on the surface, as shown in Figure 2(c). With a pulsed light irradiating on the film surface, the top surface is heated fleetly due to the light absorption, and a temperature gradient is developed, thus a thermoelectric voltage is produced in each junction. Due to the large number of junctions, the total induced voltage is very high, and the time response is very short since the distance for the carriers to move is very short.

Figure 3 shows tilting angle dependence of the LITV peak values measured in the YBCO films grown on the $SrTiO_3$ (STO) substrate. The results indicate clearly that $\sin(2\alpha)$ relation between the peak value of induced voltage and the tilting angle of the substrate is followed. Due to the difficulty in growing high-quality YBCO film on the substrate with high tilting angle, the exception of the sample grown on 20° tilted substrate does not increase with the increase tilting angle any more. ΔT depends on the incident photon fluency and the absorption of the film for the corresponding photon energy. High absorption and small penetration of the light in films lead to large ΔT and thus large induced voltage. The longer the illuminated film length *l*, the larger the induced voltage, that is, the more atomic scale thermocouples contributes to the thermoelectric signals. The thinner the film thickness (smaller *d*), the larger the induced voltage, this is correct when the films are relatively thick. However, the description in (2) is proved to be unreasonable at very thin films. Figure 4(a) shows the LITV peak values versus different thickness in YBCO films grown on STO [5]. The increase of the peak value with reducing thickness is followed above 250 nm, but the peak value undergoes a reduction below 250 nm, this dependence cannot be simply ascribed to the loss of the perfection of the thermopile arrangement. To explain this abnormal behavior, an improved model has been derived to describe the LITV mechanism. We would like to discuss this in the following.

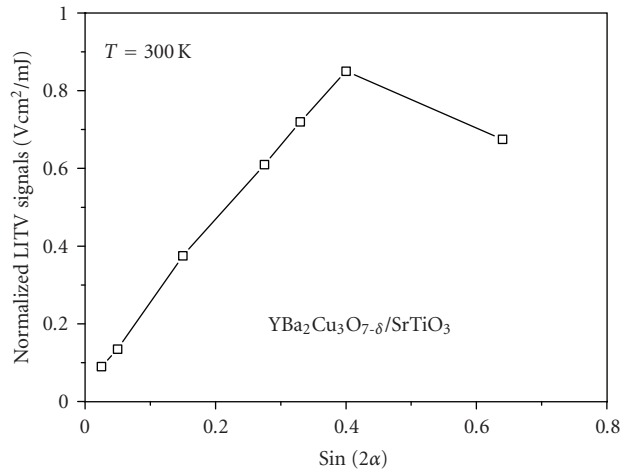

Figure 3: Measured LITV signals versus tilting angle of the substrate on which films are grown. The deviation from linear relation of last point is due to the poor film quality grown on the lager lattice mismatched substrate.

In order to correlate the material parameters to the induced voltage and the device performance, a new equation has been derived based on a plane heat source and cascade power net model [12]:

$$U(t) = \frac{\alpha_0 El\sin(2\alpha)}{4d\rho c_0\sqrt{\pi Dt}}(S_{ab} - S_c)\left(e^{-\delta^2/4Dt} - e^{-d^2/4Dt}\right), \tag{3}$$

where $U(t)$ is time-dependent LITV signal, α_0, ρ, δ, c_0, and *D* are the absorption coefficient, density, light penetration depth, specific heat, and thermal diffusivity of the film material, respectively. *E* is the energy of the incident pulsed laser integrated over the pulse duration, and all other parameters share the same definition with that. This formula provides three important results. Firstly, the peak of LITV signal is no more monotonic variation with the thickness *d*, in fact, an optimum thickness d_m which is corresponding to a maximum peak of the induced signal does exist. Secondly, to achieve a fast time response, materials with small thermal diffusivity *D* should be selected. This is totally reasonable within the frame of this new mechanism, and the response time now can be calculated quantitatively based on this formula. Thirdly, the LITV signal is affected by the light absorption of the film materials. Large absorption of the materials implies larger induced voltage. If a small penetration depth δ for the incident light is fulfilled, then both large voltage and fast time response can be achieved at the same time. On the other hand, Wang et al. has deduced the function of deciding the optimum thickness of film materials by using them differential equation of (3) and some suitable boundary conditions [17]. With inputting the material parameters of YBCO film, one can obtain the calculated peak value *Up* as a function of *d*, as shown in Figure 4(b). It is found that the optimum thickness of YBCO film for producing the maximum *Up* is about 215 nm. The calculations agree with the LITV experiments very well. As a result, based on (3) and its derivative equations, it

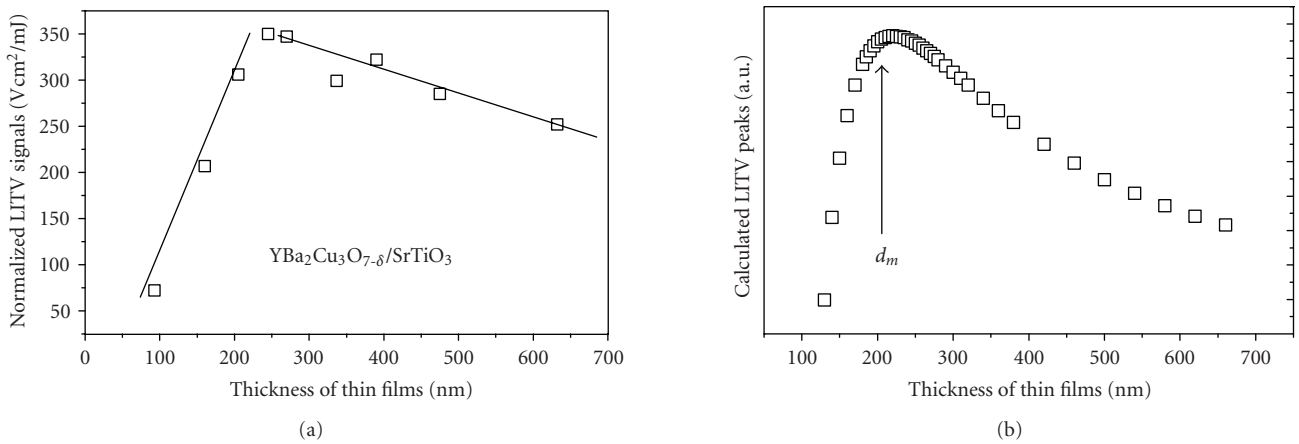

Figure 4: (a) The measured and (b) calculated LITV signals from YBCO thin films of different thicknesses are compared. The solid lines in (a) are only used to guild eyes. Both the results show there is an optimum thickness for producing the largest LITV signal.

Table 1: The parameters of materials obtained by fitting the measured LITV curves using (3).

Parameter	$S_{ab} - S_c(\mu V/K)$	D (m^2/s)	Δ (nm)	d_m (nm)
YBCO	10	7×10^{-7}	96.8	215
LCMO	0.22	7.8×10^{-9}	116.2	196

becomes easier for one to select suitable materials to design a light detector in a specified spectral range with desired time response and sensitivity [16–20].

According to the LITV experiments under different perturbations, one can obtain some thin film properties, which may not be easily measured from the bulk value. Figure 5 shows the experimental and calculated LITV signals of the YBCO thin films. The film parameters of YBCO and $LaCaMnO_3$ obtained from the fitting process are listed in Table 1.

According to Mott's band theory for non- or weakly interacting electrons, the Seebeck coefficient is expressed as [21]

$$S = -\left(\frac{\pi^2}{3}\right)\left(\frac{K_B^2 T}{e}\right)\left\{\frac{\sigma'(E_F)}{\sigma(E_F)}\right\}, \quad (4)$$

where $\sigma(E_F)$ is the conductivity at Fermi level, and $\sigma'(E_F) = (\partial\sigma/\partial E)|_{E_f}$, K_B and e are Boltzmann's constant and the elementary charge, respectively. As an approximation, (4) in most of metallic and insulating system can be expressed as $\Delta S/S \sim \Delta\rho/\rho$. It suggests that there is a close relation between the Seebeck coefficient and the resistivity: the larger the resistivity, the larger the Seebeck coefficients. Equation (4) provides the basic relation between the LITV effect and the physical properties of the strong corrected electronic materials, especially the anisotropic transport property, which is valuable information for studying the mechanism of HTSC and CMR materials. On the other hand, it also offers the important hints to seek the more effective ATL materials, since high anisotropy in conductivity links with high Seebeck anisotropy.

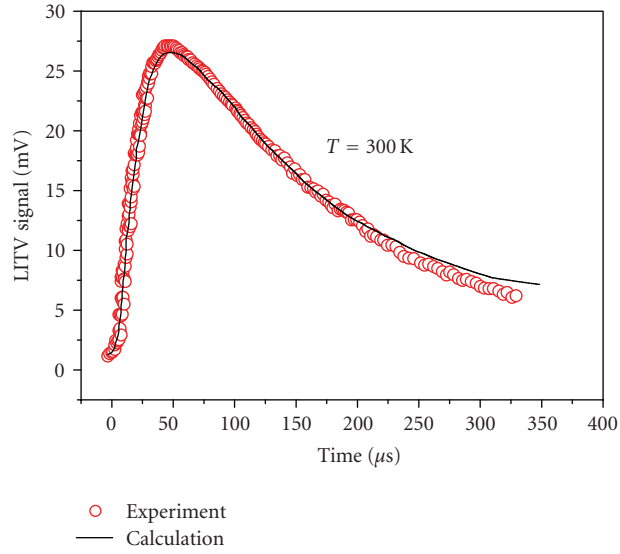

Figure 5: The measured and calculated time response curve from YBCO thin films, which demonstrate the new formula is reasonable good in describing the time dependence of the induced voltage. The obtained parameters from the fitting are listed in Table 2.

3. ALT MATERIALS

The ALT behavior is firstly observed in high T_C superconductor oxide YBCO [1]. Later, other HTSC materials, such as doped YBCO, $Bi_2Sr_2CaCu_2O_8$, $Tl_2Ba_2CaCu_2O_8$, and so forth, are studied and all of them demonstrate ALT property, only the amplitude and time response of these induced voltages are discrepant in different materials. These oxides are known as highly anisotropic due to the special layer structure. However, they are not stable in normal environment. Therefore, it is very interesting to search more practical materials.

The experimental procedures for investigating ALT materials are composed of two steps: the film preparation and the LITV measurements. The films are grown on vicinal cut

Table 2: A recapitulative comparison among the different types of photodetectors.

Parameter	Photon counting (Semiconductors)	Bolometers	ALT devices (LITV signal)
Spectral range	Narrow	Broad	Broad
Response time	Fast (ps)	Slow (ms)	Fast (sub-ps to ns)
Sensitivity	high	high	good
Bias	need	need	Do not need
Working temperature	≤300 K	45–110 K	≥280 K

substrates by pulsed laser deposition (PLD). Targets used are synthesized by solid-state reaction or coprecipitation, and can be characterized using X-ray diffraction, and other methods. The selection of substrates depends on the lattice parameter of the films to be grown on them. The most frequently used substrates are single crystal $SrTiO_3$ (STO), $LaAlO_3$ (LAO), Si, $LaSrGaO_4$, and MgO, and so forth. The selected films have been characterized by using X-ray, Raman, TEM, and other techniques to ensure that they are single phase grown on substrates. High-quality films are patterned using typical photolithography technique, and after the application of electrodes, one can directly measure the LITV signals. Two LITV measurement methods can be used according to the light source: pulsed laser or continuous-wave light sources [10, 20]. We first report the results of CMR thin film with ABO_3 structure, and then that of other new materials.

3.1. ABO_3-type thin films

At the beginning, it was a surprise to observe the LITV signal in $La_{0.67}Ca_{0.33}MnO_3$ thin film grown on vicinal cut STO substrates, since no transport anisotropy is expected in such manganites due to their cubic structure and showing paramagnetic phase above T_C. However, the signal is robust and also observed at several other doping levels. We prepared the films on substrates cut at different tilting angles to check whether these signals were induced by thermoelectric effect. Figure 6 shows the LITV obtained from Ag-doped $LaCaMnO_3$ thin films grown on LAO. It is clear that $\sin(2\alpha)$ relation is followed the large tilting angle of substrate, the larger peak of LITV signal. Therefore, the physics origin of these signals can be assigned to anisotropic Seebeck effect, and the signals were thermoelectric voltages. These experiments have demonstrated that these CMR thin films are a new type of ALT material other than high T_C superconductors. Two arisen questions then have to be answered. Firstly, whether do other manganite films with different compositions or doping levels possess strong LITV signal, so that one can apply these new materials. Secondly, why do these thin films show anisotropic transport properties. Inspired by the discovery, systematic experiments were performed, including that on different doping levels and dopant types.

In the doping experiment of $La_{1-x}Ca_xMnO_3$ system, it is revealed that the decrease in the doping level of Ca leads to a large induced voltage. According to the phase diagram, it is found that the crystal structure change from cubic to orthorhombic with the reduction of doping level x.

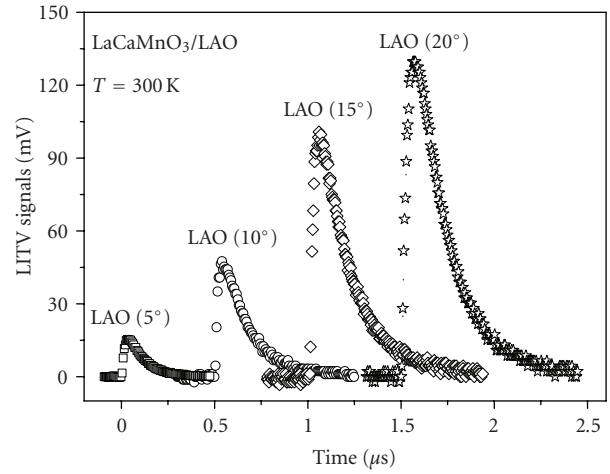

Figure 6: The LITV signals of Ag-doped $LaCaMnO_3$ thin films grown on different tilting angle $LaAlO_3$ substrates, which demonstrate that the induced voltages are due to thermoelectric anisotropy.

Therefore, a large structural anisotropy can be expected. On the other hand, less doping also changes the magnetic order from ferromagnetic to A-type antiferromagnetic, this process may facilitate the anisotropic transport of electrons at the same time. Another interesting experimental result arises from films grown on different types of substrates. Figure 7 shows the LITV signals from $LaCaMnO_3$ thin films grown on STO and LAO substrates with the same tilting angle and prepared using identical PLD conditions. The result reveals that the strains due to the mismatch between the lattice parameters of the substrate and the films grown on it have strong influence on the induced thermoelectric voltage.

Except for the $La_{1-x}Ca_xMnO_3$ thin films, several other doped manganites CMR thin films have been tested and all show similar effect, such as $LaSrMnO_3$, $LaCaSrMnO_3$, $LaPbMnO_3$ (LPMO), and $LaBaMnO_3$ [22–25]. We also synthesized cobaltite and other transition metal oxides with perovskite structure, which also demonstrate ALT properties. One typical example is the $La_{0.5}Sr_{0.5}CoO_3$ grown on vicinal cut LAO substrates. $La_{0.5}Sr_{0.5}CoO_3$ is a conductive perovskite oxide and used as electrode in fuel cell and buffer layer to grown lead-zirconate-titanate (PZT) thin films on Si substrate. We found that the time response of $La_{0.5}Sr_{0.5}CoO_3$ thin films is extremely fast [18]. The half width of the response curve is almost the same as the duration of the incident-pulsed laser, as shown in Figure 8(b). Considering

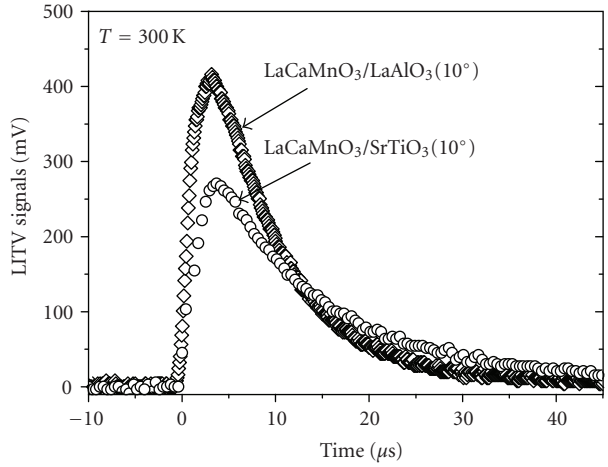

Figure 7: The influence of different substrate ($LaAlO_3$ versus $SrTiO_3$) on the LITV signals. The $LaCaMnO_3$ thin films as the samples are used in the measurements.

the limitation of the measuring method, the real time response should be in the order of picoseconds.

The fast time response of LITV in $La_{0.5}Sr_{0.5}CoO_3$ results apparently from the high-thermal diffusivity, as described in (3). In case of requirement of fast time response applications, $La_{0.5}Sr_{0.5}CoO_3$ would be a good candidate.

3.2. Ruddlesden-Popper family

Most of the ABO_3-type CMR thin films belongs to the so-called infinite layer or 113 member of Ruddlesden-Popper family, in which the anisotropy is relatively small due to their cubic structure. Therefore, it would be interesting to test other member of Ruddlesden-Popper family. One of the examples is $La_{2-x}Sr_xNiO_4$ (214 structure) grown on vicinal cut substrates [24]. Large LITV signals have been measured. The first observation of LITV from this compound further enlarges the range for seeking the more effective ALT materials. Comparing with 113 configuration, the 214 structure demonstrates large anisotropic conductivity. Hence large LITV signals can be expected. On the other hand, besides the cuprates, manganites, and cobaltite, $La_{2-x}Sr_xNiO_4$ is the first nickelate material which exhibits LITV effect. Other members of Ruddlesden-Popper family of HTSC oxides have been measured, and all the materials show high LITV signals [6–8].

3.3. Multilayer thin films

It is well known that man-made superlattices show strong anisotropy in conductivity. Is there the similar anisotropy in Seebeck tensors according to (4)? Following this question, multilayer thin films were prepared by PLD. The samples were composed with different periods (n) $YBa_2Cu_3O_{7-\delta}$ and $LaPbMnO_3$ (YBCO/LPMO) combination. The thickness of each YBCO and LPMO layer was kept at 9 and 6 nm in these multilayer samples, respectively.

The first group multilayer thin films is grown on vicinal cut LAO substrates with the tilting angle of 0°, 5°, 10°, 15°, and 20° between the surface normal and c-axis by pulsed laser deposition technique. Details of the deposition process can be found in our publication [25]. As shown in Figure 9(a), the experiments results demonstrate clearly that the larger the tilting angles the higher the induced voltages. Accordingly, our expectation has been confirmed in this experiment that the observed effect originates from Seebeck effect. Furthermore, the LITV signals are much larger than that of the individual single layer samples with identically total thickness. The YBCO/LPMO superlattices in the second group were deposited on LAO substrates with same tilting angle (10°), but with different number of period as 7, 10, 15, and 20, respectively. The LITV signals of these multilayer thin films with different periods have been presented in Figure 9(b). In order to make a comparison, the LITV signals of YBCO and LPMO single layer films with identical preparation process and measuring condition are also shown in Figure 10. It is evident that the peak value from multilayer YBCO/LPMO sample (20 periods) is about 7 and 34 times larger than that of YBCO and LPMO single-layer films, respectively.

It is known from (2) that the key factor for influencing the induced voltages is the anisotropy of Seebeck tensor ($S_{ab} - S_c$). In the superlattice or multilayer film systems, it is difficult to predict the laser absorption, penetration depth, and specific heat which also directly affect the LITV signal, due to the large variation of these parameters in these special systems. Therefore, one has to focus on the possibility of the enhancement from the discrepancy of Seebeck tensor ($S_{ab} - S_c$). For the multilayer structure, it is obvious that the carrier transportation exhibits high anisotropy. In the layer plane, the conductivity is rather high; while in the perpendicular direction, that is relative smaller. With the increase of the period number, the probability of carrier scattering enhances due to the increase of the defects from the interface. As mentioned in (4), large resistivity leads to large Seebeck coefficient, therefore, the large ($S_{ab} - S_c$). Another key influencing factor is the thermal conductivity. There are numbers of discussion on the thermal conductivity of some manganites with layered structures [26, 27]. Simkin and Mahan have calculated the phonon contribution to thermal conductivity (D) in superlattices. It has been concluded that D is closely related to the number of superlattice periods (n) and the phonon mean-free path. The heat conduction in perpendicular direction of the layer plane is highest for the samples with small n, and rapidly decreases with n increases, after reaching a minimum within the range of n = 7–15, increases again. The smaller the mean-free path of phonon implies the smaller the n, at which the minimum thermal conductivity is achieved. In superlattice materials, the electrons are confined for certain situation, and the phonons are scattered at the interfaces. Therefore, the high-thermoelectric figure of merit (ZT) is expected, and indeed the ZT as high as 2 to 3 have been measured in several experiments [28–30].

The possible enhancement of ($S_{ab} - S_c$) may originate from the stressed lattices. According to X-ray diffraction,

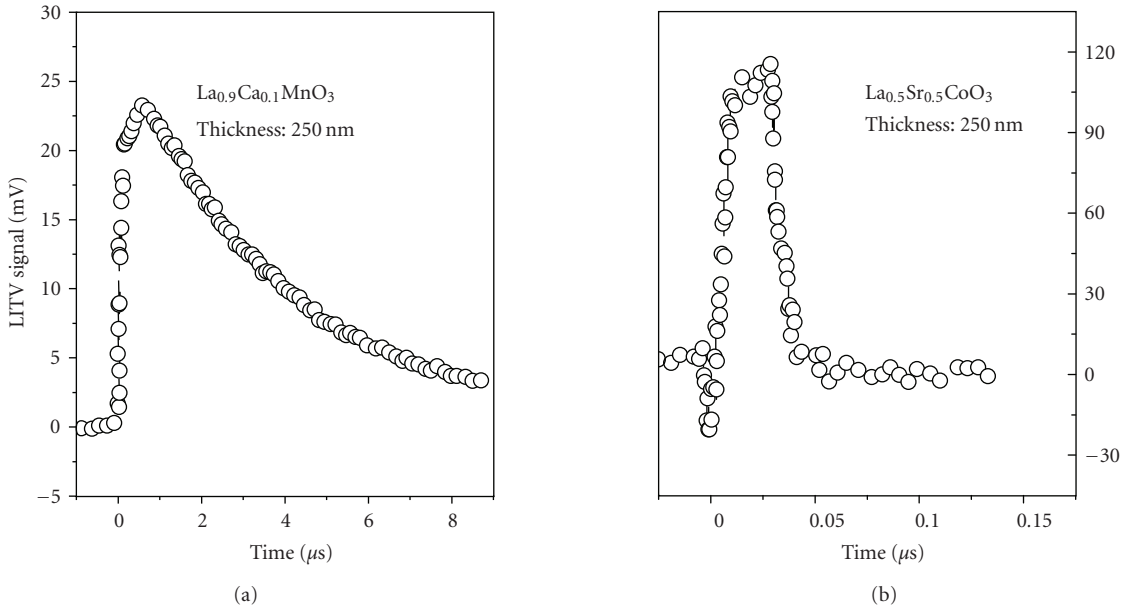

FIGURE 8: (a) The LITV time response curves from $LaCaMnO_3$ and (b) $LaSrCoO_3$ thin films. It is shown that the time response of $LaSrCoO_3$ is very fast (ps-ns) due to its highe conductivity.

both YBCO and LPMO films are compressively stressed in *ab* plane due to the smaller lattice parameter of LAO substrate. Therefore, the lattice parameters in *c*-direction were enlarged assuming preservation of the volume of the unit cell. The large mismatch and the sandwiched structure can keep this strain in the whole sample. This leads to the variation of intrinsic properties of each component films. Due to the strain effects, the stressed YBCO and LPMO films must show different transport properties, this has been verified by several experiments [16–19, 31].

In a word, there is a huge variety of strong correlated electronic materials which are not yet studied from the viewpoint of their ALT properties. According to our limited research so far, it is clear that most of the materials with layered structure demonstrate ALT properties. For the first time, an enhanced LITV signal from multilayer oxide thin films with a superlattice-like structure is observed. Compared with single-layer film of YBCO or LPMO, the LITV signals of the multilayer sample (the YBCO/LPMO structure with 7 periods) have been enhanced for several times than those obtained in YBCO and LPMO single films. This new observation is interesting for studying the transport properties in superlattice-like multilayer thin films. The unusual enhancement of the light-induced voltages in these multilayer films is possibly related to the large Seebeck anisotropy and the reduction of thermal conductivity in superlattice-like structures. The investigation of these materials and thin films provides candidates for different applications, such as light detection at different wavelengths or time responses. On the other hand, the measured LITV signals from the superlattices-like structures provide information on the anisotropic transport property, which are hard to obtain by other experiments.

4. APPLICATION

Two practical applications have been put forward and tested with the ALT materials. One is light and heat detection, and the other is local cooling based on the reverse of the Seebeck effect, the Peltier effect.

The thermoelectric response of an ALT material has a linear dependence on absorbed radiation power. Therefore, a radiation detector was designed and tested [14, 18–20]. To compare the ALT detectors with those fabricated by other materials, Table 2 lists the main parameters for three types of detectors. Due to the broad absorption of the black surfaces of most of the ALT materials, the LITV detectors can work in broad spectrum range. The experiment shows that these detectors can response from ultraviolet to middle infrared. According to (3), the time response depends on the thermal diffusivity D and the penetration depth δ. By proper selecting the materials responded at special wavelength, response time from micro- to picoseconds is easy to be realized. Other advantages of this type of detectors consist in that they show good performance at room temperature without any biases.

Considering that the importance for fabricating the devices with fast time response and high sensitivity, one can define a device figure of merit (F_m) to describe the performance of the LITV detector [18]:

$$F_m = \frac{U_P}{\tau}, \tag{5}$$

where U_P and τ are the peak value of induced voltage and the full width at half maximum of the response curve of the induced voltages. Therefore, synthesizing and searching for materials with high LITV sensitivity and fast time response at the same time, namely, higher F_m is interesting.

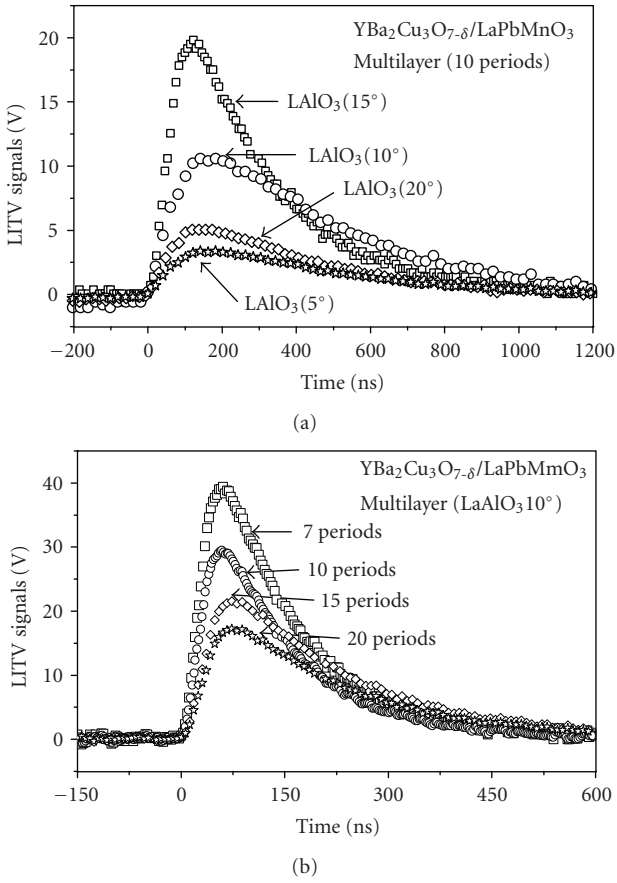

Figure 9: (a) The LITV signals from the multilayer YBCO/LPMO thin films with 10 periods grown on different vicinal cut substrates. From these curves, it has been confirmed that the LITV signals originate from thermoelectric anisotropy. (b) The multilayer thin films with different period number n grown on vicinal cut $LaAlO_3$ (10°) substrates.

Table 3: The measured conductivity δ, peak values of LITV signals U_p, time response τ, and the calculated figure of merit for different Ag-doped $La_{0.6}Pb_{0.4}MnO_3$ films grown on $LaAlO_3$ substrates with 15° angle cut.

Ag-doping level (wt%)	δ (S/cm)	U_p (mV)	τ (ns)	F_m
0	313.8	25	140	0.18
2	567.7	35	106	0.33
4	1302.1	43	80	0.53
6	2125.9	38	65	0.58
8	901.9	48	100	0.48
10	749.4	20	126	0.16

We have prepared Ag-doped $La_{0.6}Pb_{0.4}MnO_3$ (Ag-LPMO) thin films by means of PLD, and investigated the doping level effect on the LITV amplitude. By optimizing the doping level of Ag, it is found that the F_m of the LITV device is improved substantially.

The LITV signals of Ag-LPMO films with different Ag doping levels are shown in Figure 11. The U_P value firstly increases with the increase of Ag doping level, then reaches

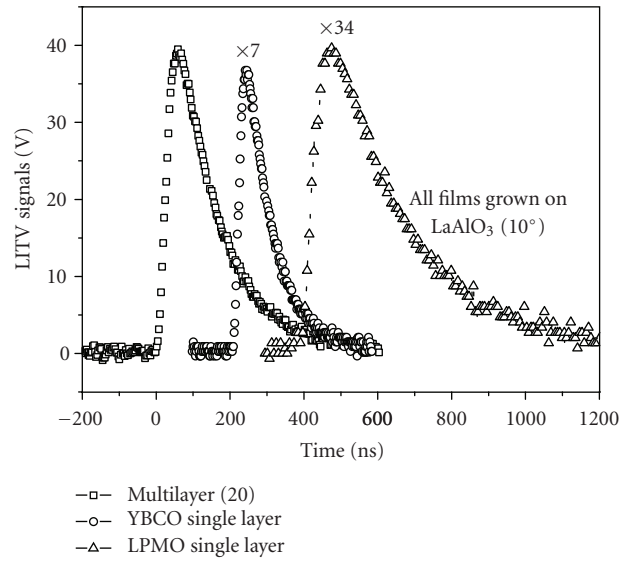

Figure 10: The LITV signals of the YBCO/LPMO multilayer film with 20 periods, the 400 nm thick $YBa_2Cu_3O_{7-\delta}$ thin film, and the 400 nm thick $LaPbMmO_3$ films, respectively. The samples are fabricated and measured at the identical experimental conditions.

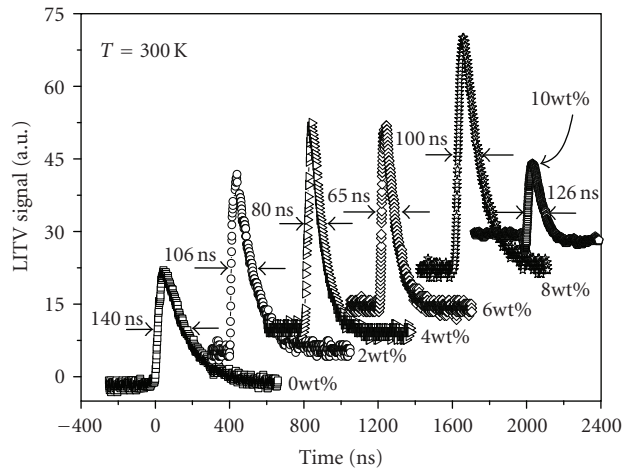

Figure 11: Time dependent laser induced voltage curves obtained from different Ag-doped $La_{0.6}Pb_{0.4}MnO_3$ films grown on vicinal cut $LaAlO_3$ (15°) substrates. These samples are also fabricated and measured at the same experimental conditions. It is shown that the figure of merit of the LITV device can be greatly improved with proper doping level.

a maximum at doping level of 4–6 wt%, finally decreases. At the same time, the time response τ varies with an opposite way, reduce first and then increase. According to (5), one can calculate the F_m values of these devices. Table 3 lists the measured U_P, τ, and the calculated F_m at different Ag-doping levels. It is evident that F_m value can be enhanced to several times by optimizing doping level of Ag.

There are lots of discussion on the enhancement of the ZT of thermoelectric materials, and several new concepts to obtain materials with ZT higher than 1 have been reported

[28–30]. To form materials with "phonon glass and electron crystal" behavior become the central issue to realize large ZT, namely, high-electronic conductivity and low-thermal conductivity. Doping with monovalent ions, such as Ag, either in the lattice or at grain boundary, always enhances electronic conductivity. At the same time, the inhomogeneity is induced by doping Ag because the Ag ions form the centers of phonon scattering. Therefore, doping with Ag in the $LaPbMnO_3$ films can enhance the ZT, and this may be an effective method for other material system as well.

The reverse effect of Seebeck is Peltier effect, in which a thermoelectric cooling can be realized by simply applying electric current. In an anisotropic material, an applied electrical current density J_e can produce a Peltier heat flow J_h, which is described by

$$J_h = P \cdot J_e, \tag{6}$$

where P is the Peltier tensor, related to Seebeck tensor S, defined as $P = S \cdot T$. The largest temperature difference ΔT_m realized in this effect depends on the thermoelectric figure of merit ZT and is expressed as

$$\Delta T_m = \frac{(ZT)^2}{2}. \tag{7}$$

The cooling effect of ALT materials was firstly observed in YBCO bulk [32]. Recently, more effective cooling effect was realized in a Pb-Bi_2Te_3 multilayer structure [33]. By applying a current in film plane, temperature difference up to 22 K has been observed between top and bottom sides of the sample. The cooling experiments on ALT materials are just launched. However, the renewed interests in microcooling for various applications are pushing the related investigations. The advantages of the type of cooling are easy to realize, without moving parts, matching well with plane technology, and so on.

5. PHYSICAL MECHANISMS AND OPEN QUESTIONS

All crystalline solid materials are composed of atomic layers, therefore, they should have ALT behavior and can be the candidates for the application and LITV measurements. So far, only few have been studied. Large unreached area remains to be explored. The studies of HTSC and CMR thin films have put forward several questions which should be answered, for example, why there is anisotropy in CMR thin films with cubic or quasicubic crystal structure? Even more interesting is that the LITV signals are recorded at temperature above T_C, the films are in paramagnetic phase. What information can be followed by analyzing the LITV signals at different applied perturbations? Clear answer of these questions involves in the mechanisms of charge and phonon transport in the strongly correlated electronic systems, which are also the hot points of condensed matter physics.

We now discuss the origin of LITV signals from CMR thin films and try to answer the origin of the anisotropy in these films. In fact, the existence of LITV signals is closely linked with the mixed phases of the complicated system.

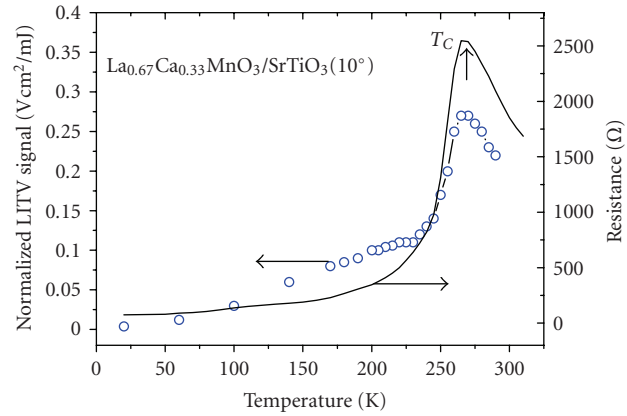

FIGURE 12: Temperature dependence of LITV signals (separated dots) and resistance (solid line) of $LaCaMnO_3$ thin film. It is shows that the amplitude of LITV signals is relative strong around T_C.

Assuming that there are two competing phases near T_C in CMR materials [34–36], the ferromagnetic metallic (FMM) and charge-ordered antiferromagnetic (COAF) insulating phase, the total induced voltage based on (2) is composed of the contribution of the two:

$$U_P = A[S^1_{an}(1 - C) + S^2_{an} \cdot C], \tag{8}$$

where U_P is the peak value of induced voltages. S^1_{an} and S^2_{an} are defined as $(S_{ab} - S_c)$ in COAF and FMM phases, respectively. C is the concentration of FMM phase, which can be evaluated from the measured temperature or applied magnetic fields dependence of magnetization (M) and expressed as $C(H, T) = M(H, T)/M_{\text{sat}}$ [37]. A is a constant related to the geometric dimension of the sample and the temperature gradient in the materials produced by the pulsed laser, which is temperature independent in the first approximation. Considering no other phase transition and only the two phases playing important role, two extreme cases can be discussed. At the temperature range of $T \gg T_C$, the FMM phase disappears, C approaches to zero correspondingly. Based on (8), one can evaluate high-temperature Seebeck anisotropy of COAF phase: $S^1_{an}(hT) = U_P(hT)/A$. While in the case of $T \ll T_C$ the contribution of COAF phase is negligible, small one can obtain Seebeck anisotropy of FMM phase at low temperature $S^2_{an}(lT) = U_P(lT)/A$. Figure 12 shows the LITV signals obtained from $La_{0.67}Ca_{0.33}MnO_3$ thin films grown on STO substrates [14]. According to the above analysis and estimation, the Seebeck anisotropy of COAF phase at high temperature is $S^1_{an}(hT) = 0.2/A$, for FMM phase at low temperature is $S^2_{an}(lT) = 0.01/A$, and a ratio $S^1_{an}(hT)/S^2_{an}(lT) = 20$ was obtained.

These results are reasonable. For the FMM phase, the structure of $La_{0.67}Ca_{0.33}MnO_3$ is cubic, and the anisotropy is small, while the COAF phase is possibly noncubic [34], this implies that a large anisotropy can be expected. In fact, it is well known that the Seebeck coefficient is closely related to the conductivity. According to (4), the larger the resistivity the larger the Seebeck coefficients. For the two coexistent phases near and above T_C, the FMM phase

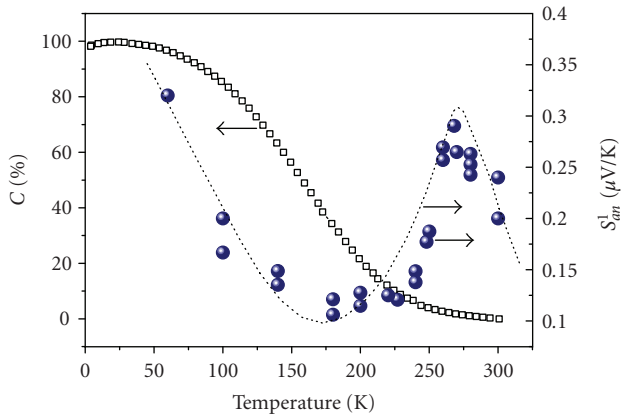

Figure 13: Temperature dependence of Seebeck coefficient anisotropy ($S^1_{an} = S_{ab} - S_c$), deduced from measured LITV signal based on two phases model. The dot line is only used to guide eyes.

is the one with higher conductivity and lower resistivity, therefore the Seebeck coefficients are relative smaller. In addition, due to the cubic structure, the anisotropy should be further suppressed at the same time. On the contrary, the COAF phase is insulating (large resistivity), then a large Seebeck coefficient is expected, and even a large structural anisotropy occurs. With this argument and also considering the evaluated values and the ratio $S^1_{an}(hT)/S^2_{an}(lT) = 20$, one can further simplify (8) as $U_P = AS^1_{an}(1 - c)$. This approximation is valid at temperature near and above T_C. Since C can be evaluated from magnetization measurements accordingly, and based on the measured LITV temperature dependence [8], the temperature dependence of S^1_{an} is easily estimated. Figure 13 shows the obtained $S^1_{an} - T$ dependence from experiments, together with the used $M(T)$ curve. Based on these results, the concentration of FMM phase can be easily estimated. With the decrease of temperature, it is shown that the difference of the Seebeck coefficients $S^1_{an} = (S_{ab} - S_c)$ or the anisotropy of the resistivity in COAF phase increases firstly. After it reach a maximum at around T_C, then the S^1_{an} decreases again. Since there are significant LITV signals measured above T_C, we would like to emphasize that the anisotropic Seebeck coefficients are robust. Therefore, an anisotropic transport behavior can be definitely observed above T_C in paramagnetic phase of $La_{0.67}Ca_{0.33}MnO_3$ thin films. This is unexpected, since the sample is cubic or quasicubic in terms of its structure, and magnetically is in paramagnetic phase, both factors should not lead to anisotropic transport properties. In fact, the temperature-dependent Seebeck coefficient has been measured at temperature near and above T_C in $La_{0.67}Ca_{0.33}MnO_3$ bulk by Jaime et al. [37], which is an isotropic value, and demonstrated qualitatively the same temperature behavior as the deduced S^1_{an} from LITV measurements. This means that the difference of $S_{ab} - S_c$ is roughly proportional to the absolute value of S as a function of temperature. The interesting point is that the obtained anisotropic components should be correlated to the structural anisotropy as well as the conductivity anisotropy of a possible COAF phases. Recently, there were a number of experiments which reported the measurement of Seebeck coefficients from $Pr_{0.67}D_{0.33}MnO_3$ (D = Ca, Sr, Pb, and Ba) by Venkataiah et al. [38, 39], $La_{0.7}Sr_{0.3-x}Ag_xMnO_3$ by Battabyal and Dey [40], these results demonstrated similar temperature behavior as the one observed in [37]. However, all of the results of their samples are obtained in the bulk materials, and less information on the anisotropy of the thermoelectric effects is given. Furthermore, there is no discussion on the contribution of the competing phase in these materials. Therefore, it is hard to tell which phase is responsible to the anisotropy.

There are several possible phases coexistent with the FMM phase above T_C [41–43]. Figure 14 shows the spin structure in A, C, and G types of antiferromagnetic phases, together with a ferromagnetic (F) and newly proposed CE, E, and C_xE_{1-x} types of charge-ordered antiferromagnetic phases. The parent compounds of doped $La_{0.67}Ca_{0.33}MnO_3$ are $LaMnO_3$ and $CaMnO_3$. The undoped $LaMnO_3$ is orthorhombic (space group P_{nma}), with magnetic ground state of A-type antiferromagnetic structure. In *a-c* plane, the alignment of spins is parallel, it indicates the configuration of two-dimensional ferromagnetism. While in the successive plane of *b* direction, the orientations of the spins are antiparallel. Therefore, the transport anisotropy has been built accordingly, that is, the electrons can move easily in the *a-c* plane, but difficultly in the *b* direction due to the antiparallel spin orientation. The other doping end is $CaMnO_3$, which is cubic in structure (space group P_{m3m}) and with magnetic ground state of G-type antiferromagnetic structure. In this phase, there is no anisotropy originated from crystal and magnetic structure. With different doping levels, the COAF phases could be a mixture of all these phases at temperature near and above T_C. The CE phase is most likely the candidate, which is responsible for an anisotropic transport property. The zigzag conductive chains are in *ab* planes, while the conductivity in *c* direction is very poor because the hopping of spin is forbidden. The E-type of COAF phase is similar to CE-type. However, the zigzag chains are composed of two parallel oriented spins. Therefore, there is also anisotropic transport property. The carrier transport may be easier in the zigzag chains than that in CE phase. Up to now, it is hard to directly correlate which phase is responsible for the measured Seebeck anisotropy. More theoretical and structural studies are required to make the question be clearer.

In summery, a new experimental method, laser induced thermoelectric voltage effect from CMR thin films, was used for the first time to reveal the transport anisotropy at temperature near and above T_C in $La_{0.67}Ca_{0.33}MnO_3$ thin film. By neglecting the contribution of FMM phase, the temperature dependence of $S_{ab} - S_c$ in COAF phase was evaluated, this dependence provides clear evidence for the existence of noncubic, highly anisotropic phase above T_C.

The results show that the Seebeck coefficients difference $S_{ab} - S_c$ in COAF phase increases firstly with the lowering temperature, and then reaches a maximum at around T_C, finally decreases again. This information is unique, and may offer great help in correlating COAF phase type as well as the mechanisms of the complicated phase competition

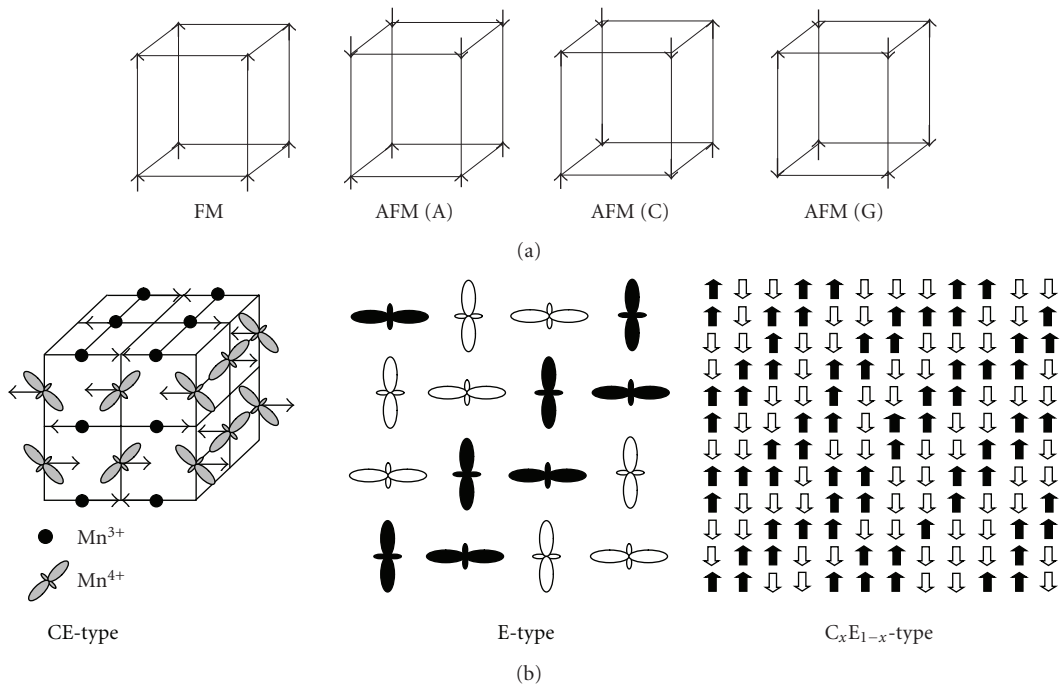

FIGURE 14: The possible antiferromagnetic phases in mixed phases of CMR materials around T_C.

and coexistence in CMR materials. In fact, similar situation is also in high T_C superconductor materials, where a T^* is defined, and little is known on the region between T^* and T_C. Therefore, LITV measurements may contribute valuable information on the anisotropic transport, and hence the physical understanding of strongly correlated electronic systems.

6. CONCLUSION

Atomic layer thermopile (ALT) materials are a new type of materials, which demonstrate novel thermoelectric property. The basic principle originates from the different transport properties in different atomic layers, this induces the anisotropic Seebeck effect. This effect can be used in light or heat detection, and local cooling based on its inverse effect. There are large amounts of materials which may exhibit ALT property, but not yet well studied. The investigations of LITV in different ALT materials provide unique information on transport properties at temperatures especially important for study the mechanism of high T_C superconductor and CMR effect.

ACKNOWLEDGMENTS

P.X. Zhang would like to thank Professor C. Wang (Yunnan University) for the fruitful discussion and technical assistance. Both authors would like to thank X.-H. Li, W.K. Lee, B. Leibold, G. Cristiani, G. Y. Zhang, H. Zhang, and L. Yu for their contributions covering various aspects of this work. The financial supports are from science foundation of China (10274026, 1999E0003Z).

REFERENCES

[1] C. L. Chang, A. Kleinhammes, W. G. Moulton, and L. R. Testardi, "Symmetry-forbidden laser-induced voltages in $YBa_2Cu_3O_7$," *Physical Review B*, vol. 41, no. 16, pp. 11564–11567, 1990.

[2] H. S. Kwok, J. P. Zheng, Q. Y. Ying, and R. Rao, "Nonthermal optical response of Y-Ba-Cu-O thin films," *Applied Physics Letters*, vol. 54, no. 24, pp. 2473–2475, 1989.

[3] H. Lengfellner, G. Kremb, A. Schnellbögl, J. Betz, K. F. Renk, and W. Prettl, "Giant voltages upon surface heating in normal $YBa_2Cu_3O_{7-\delta}$ films suggesting an atomic layer thermopile," *Applied Physics Letters*, vol. 60, no. 4, pp. 501–503, 1992.

[4] Th. Zahner, R. Schreiner, R. Stierstorfer, et al., "Off-diagonal Seebeck effect and anisotropic thermopower in $Bi_2Sr_2CaCu_2O_8$ thin films," *Europhysics Letters*, vol. 40, no. 6, pp. 673–678, 1997.

[5] P. X. Zhang, U. Sticher, B. Leibold, and H.-U. Habermeier, "Thickness dependence of the thermoelectric voltages in $YBaCuO_{7-\delta}$ thin films on tilted substrate of $SrTiO_3$," *Physica C*, vol. 282–287, part 4, pp. 2551–2552, 1997.

[6] L. R. Testartdi, "Anomalous laser-induced voltages in $YBa_2Cu_3O_x$ and "off-diagonal" thermoelectricity," *Applied Physics Letters*, vol. 64, no. 18, pp. 2347–2349, 1994.

[7] Th. Zahner, R. Förg, and H. Lengfellner, "Transverse thermoelectric response of a tilted metallic multilayer structure," *Applied Physics Letters*, vol. 73, no. 10, pp. 1364–1366, 1998.

[8] X. H. Li, *Strongly correlated oxide thin films and laser induced voltage effect*, doctorial thesis, Institute of Physics, ChineseAcademic Sciences, Beijing, China, 2001.

[9] S. Zeuner, W. Prettl, and H. Lengfellner, "Fast thermoelectric response of normal state $YBa_2Cu_3O_{7-\delta}$ films," *Applied Physics Letters*, vol. 66, no. 14, pp. 1833–1835, 1995.

[10] P. X. Zhang, G. Z. Li, X. M. Wen, Y. Zhang, and H.-U. Habermeier, "Room temperature light-thermo-detector made

of high-T-c superconductor," *Acta Physica Sinica*, vol. 7, no. 11, pp. 810–816, 1998.

[11] K. Fischer, C. Stoiber, A. Kyarad, and H. Lengfellner, "Anisotropic thermopower in tilted metallic multilayer structures," *Applied Physics A*, vol. 78, no. 3, pp. 323–326, 2004.

[12] P. X. Zhang, W. K. Lee, and G. Y. Zhang, "Time dependence of laser-induced thermoelectric voltages in $La_{1-x}Ca_xMnO_3$ and $YBa_2Cu_3O_{7-\delta}$ thin films," *Applied Physics Letters*, vol. 81, no. 21, pp. 4026–4028, 2002.

[13] P. X. Zhang, C. Wang, G. Y. Zhang, L. Yu, W. K. Lee, and H.-U. Habermeier, "$LaCaMnO_3$ thin film laser energy/power meter," *Optics and Laser Technology*, vol. 36, no. 4, pp. 341–343, 2004.

[14] Th. Zahner, R. Stierstorfer, S. Reindl, T. Schauer, A. Penzkofer, and H. Lengfellner, "Picosecond thermoelectric response of thin $YBa_2Cu_3O_{7-\delta}$ films," *Physica C*, vol. 313, no. 1-2, pp. 37–40, 1999.

[15] H.-U. Habermeier, X. H. Li, P. X. Zhang, and B. Leibold, "Anisotropy of thermoelectric properties in $La_{2/3}Ca_{1/3}MnO_3$ thin films studied by laser-induced transient voltages," *Solid State Communications*, vol. 110, no. 9, pp. 473–478, 1999.

[16] X. H. Li, H.-U. Habermeier, and P. X. Zhang, "Laser-induced off-diagonal thermoelectric voltage in $La_{1-x}Ca_xMnO_3$ thin films," *Journal of Magnetism and Magnetic Materials*, vol. 211, no. 1, pp. 232–237, 2000.

[17] C. Wang, P. X. Zhang, and G. Y. Zhang, "Optimum thickness for laser induced thermoelectric voltage effect in high T-c superconductor and CMR thin film," *Acta Physica Sinica*, vol. 53, no. 6, pp. 1727–1730, 2004.

[18] P. X. Zhang, G. Y. Zhang, H. J. Wu, et al., "Time constant of laser-induced thermoelectric voltage device made by $LaCaMnO_3$, $YBa_2Cu_3O_{7-\sigma}$ and $LaSrCoO_3$ thin films," *Transactions of the Materials Research Society of Japan*, vol. 29, no. 4, pp. 1423–1426, 2004.

[19] G.-Y. Zhang, P. X. Zhang, H. Zhang, and W. K. Lee, "Figure of merit for detectors based on laser-induced thermoelectric voltages in $La_{1-x}Ca_xMnO_3$ and $YBa_2Cu_3O_{7-\delta}$ thin films," *Chinese Physics Letters*, vol. 22, no. 9, pp. 2379–2381, 2005.

[20] W.-D. Cui, H. Zhang, G.-Y. Zhang, J.-T. Hu, Y.-N. Dai, and P.-X. Zhang, "Laser induced thermoelectric voltage of atomic layer thermopile materials," *Chinese Journal of Lasers*, vol. 34, no. 1, pp. 130–134, 2007.

[21] N. F. Mott and E. A. Davis, *Electronic Processes in Non-crystaline Materials*, Oxford University Press, Oxford, UK, 1979.

[22] Y. L. Yang, *Preparation and LITV effect of $LaSrCaMnO_3$ thin films*, M.S. thesis, Kunming Institute of Science and Technology, Kunming, China, 2005.

[23] J. L. Wang, *Conductive $LaSrCoO_3$ thin film and laser induced voltage properties*, M.S. thesis, Kunming Institute of Science and Technology, Kunming, China, 2005.

[24] Y. Yuan, H. Zhang, T. S. Tan, and P.X. Zhang, "Growth and laser induced thermoelectric voltage effect of the c-axis oriented $Ca_3Co_4O_9$ thin film on sapphire substrates," *Chinese Journal of Lasers*, vol. 35, p. 921, 2008.

[25] L. L. Xie, H. Zhang, and P. X. Zhang, "Preparation and LITV effect in $YBaCuO_{7-\delta}LaPbMnO_3$ Multilayer," *Journal of Low Temperature Physics*, vol. 29, p. 109, 2007.

[26] M. V. Simkin and G. D. Mahan, "Minimum thermal conductivity of superlattices," *Physical Review Letters*, vol. 84, no. 5, pp. 927–930, 2000.

[27] R. Venkatasubramanian, E. Siivola, T. Colpitts, and B. O'Quinn, "Thin-film thermoelectric devices with high room-temperature figures of merit," *Nature*, vol. 413, no. 6856, pp. 597–602, 2001.

[28] T. C. Harman, P. J. Taylor, M. P. Walsh, and B. E. LaForge, "Quantum dot superlattice thermoelectric materials and devices," *Science*, vol. 297, no. 5590, pp. 2229–2232, 2002.

[29] R. Venkatasubramanian, "Lattice thermal conductivity reduction and phonon localizationlike behavior in superlattice structures," *Physical Review B*, vol. 61, no. 4, pp. 3091–3097, 2000.

[30] L. D. Hicks and M. S. Dresselhaus, "Effect of quantum-well structures on the thermoelectric figure of merit," *Physical Review B*, vol. 47, no. 19, pp. 12727–12731, 1993.

[31] M. Matsukawa, M. Narita, T. Nishimura, et al., "Anisotropic phonon conduction and lattice distortions in colossal-magnetoresistance bilayer manganite $(La_{1-z}Pr_z)_{1.2}Sr_{1.8}Mn_2O_7$ ($z = 0$, 0.2, 0.4, and 0.6) single crystals," *Physical Review B*, vol. 67, no. 10, Article ID 104433, 6 pages, 2003.

[32] Z. H. He, Z. G. Ma, Q. Y. Li, et al., "Investigation of transverse Peltier effect on top-seeded melt texture $YBa_2Cu_3O_{7-\delta}$," *Applied Physics Letters*, vol. 69, no. 23, pp. 3587–3589, 1996.

[33] A. Kyarad and H. Lengfellner, "Transverse Peltier effect in tilted Pb-Bi_2Te_3 multilayer structures," *Applied Physics Letters*, vol. 89, no. 19, Article ID 192103, 3 pages, 2006.

[34] K. H. Ahn, T. Lookman, and A. R. Bishop, "Strain-induced metal-insulator phase coexistence in perovskite manganites," *Nature*, vol. 428, no. 6981, pp. 401–404, 2004.

[35] A. J. Millis, "Lattice effects in magnetoresistive manganese perovskites," *Nature*, vol. 392, no. 6672, pp. 147–150, 1998.

[36] Z.-H. Wang, G. Cristiani, and H.-U. Habermeier, "Uniaxial magnetic anisotropy and magnetic switching in $La_{0.67}Sr_{0.33}MnO_3$ thin films grown on vicinal $SrTiO_3(100)$," *Applied Physics Letters*, vol. 82, no. 21, pp. 3731–3733, 2003.

[37] M. Jaime, P. Lin, S. H. Chun, M. B. Salamon, P. Dorsey, and M. Rubinstein, "Coexistence of localized and itinerant carriers near T_C in calcium-doped manganites," *Physical Review B*, vol. 60, no. 2, pp. 1028–1032, 1999.

[38] S. Uhlenbruck, B. Büchner, R. Gross, A. Freimuth, A. Maria de Leon Guevara, and A. Revcolevschi, "Thermopower and anomalous heat transport in $La_{0.85}Sr_{0.15}MnO_3$," *Physical Review B*, vol. 57, no. 10, pp. R5571–R5574, 1998.

[39] G. Venkataiah, Y. K. Lakshmi, and P. V. Reddy, "Thermopower studies of $Pr_{0.67}D_{0.33}MnO_3$ manganite system," *Journal of Physics D*, vol. 40, no. 3, pp. 721–729, 2007.

[40] M. Battabyal and T. K. Dey, "Seebeck coefficient in polycrystalline $La_{0.7}Sr_{0.3-x}Ag_xMnO_3$ pellets: analysis in terms of a phase separation model," *Journal of Physics: Condensed Matter*, vol. 18, no. 2, pp. 493–505, 2006.

[41] E. Dagotto, "Open questions in CMR manganites, relevance of clustered states and analogies with other compounds including the cuprates," *New Journal of Physics*, vol. 7, no. 1, pp. 67–95, 2005.

[42] Y. Tomioka and Y. Tokura, "Global phase diagram of perovskite manganites in the plane of quenched disorder versus one-electron bandwidth," *Physical Review B*, vol. 70, no. 1, Article ID 014432, 5 pages, 2004.

[43] Ch. Renner, G. Aeppli, B.-G. Kim, Y.-A. Soh, and S.-W. Cheong, "Atomic-scale images of charge ordering in a mixed-valence manganite," *Nature*, vol. 416, no. 6880, pp. 518–521, 2002.